Applied Ocean Research 162 (2025) 104727

Contents lists available at ScienceDirect

Applied Ocean Research

journal homepage: www.elsevier.com/locate/apor

Research paper

Rip current likelihood as a function of incident wave conditions for different bathymetries

Junwoo Choi [a,*], Steve Elgar [b], James T. Kirby [c]

[a] River and Coastal Research Division, Korea Institute of Civil Engineering & Building Technology, Goyang 411-712, South Korea
[b] Applied Ocean Physics & Engineering Department, Woods Hole Oceanographic Institution, MA 02543, USA
[c] Center for Applied Coastal Research, Department of Civil and Environmental Engineering, University of Delaware, Newark, DE 19713, USA

ARTICLE INFO

Keywords:
Rip currents
rip-current likelihood
Numerical simulation
FUNWAVE
Surf currents

ABSTRACT

The likelihood of rip currents as a function of water depth (tidal level), incident wave height, period, direction, and spectral spreading in both frequency and direction is investigated with a Boussinesq numerical model (FUNWAVE) for alongshore uniform, moderately variable, and strongly variable bathymetry, providing two-dimensional probability distributions of rip-current occurrence along the coast. The simulations suggest that over strongly irregular alongshore bathymetry rip-current likelihood increases with longer wave periods and narrower directional spectra. In contrast, over more uniform alongshore bathymetry, rip current likelihood increases with shorter wave periods and broader directional spectra. The simulations suggest that as bathymetric variability increases, the effects of different incident wave fields decreases.

1. Introduction

Rip currents pose a serious threat to beachgoers worldwide, resulting in dozens of deaths in the U.S. and Australia (Gensini and Ashley, 2009; NOAA, 2022a; SLS, 2022). Rip currents typically form when topography, wave-wave interactions, and instabilities result in a significant alongshore non-uniformity in the wave-induced momentum flux (Bowen, 1969; Tang and Dalrymple, 1989; Dalrymple et al. 2011). These currents can occur at any coast where waves break unevenly along the shore, and predicting their occurrence remains a challenging issue in ocean forecasting.

Variations in coastal topography can lead to alongshore non-uniform wave heights and breaking patterns, resulting in the formation of persistent, topographic-induced eddies and rip currents. This coastal variability within the breaking zone can generate rip currents under incident wave conditions that may have been transformed by alongshore topographic changes in the offshore areas (Castelle et al. 2016b; Shin et al. 2013). Topographically controlled rip currents usually remain stationary over wave time scales, depending on the characteristics of the underlying bathymetry. However, the flow field also can display pulsations at low frequencies, particularly within the infragravity range (Haller and Dalrymple, 2001; MacMahan et al. 2004). Furthermore, rip currents induced by offshore topographic variations can experience shifts in both timing and location (Yoon et al. 2013). The generation and movement of rip currents, including the energy of very low-frequency (VLF) motions, are strongly influenced by changes in incident wave conditions and coastal topographic variations (Akan et al. 2020; O'Dea et al. 2021; Uchiyama et al. 2017).

Although previous studies have analyzed rip current characteristics under specific bathymetry and specific wave conditions, such as wave height (Dalrymple et al. 2011), direction (Moulton et al. 2017), and directional spreading (Spydell and Feddersen, 2009; Suanda and Feddersen, 2015), comprehensive evaluations that account for variability due to a range of incident wave conditions (Dusek and Seim, 2013a, b) and topography together (Choi et al. 2013) are rare. To advance the ability to predict rip currents, it is crucial to assess the relative possibility of a dominant rip current forming under different incident wave conditions (e.g., wave height, period, direction, spectral spreading, tidal elevation) at a specific natural bathymetry, regardless of whether the rip current is persistent or transient (Choi 2025). A method for quantifying the likelihood of rip current occurrence for a range of wave parameters within FUNWAVE simulations was developed through numerical simulations (Choi 2025) allowing investigation of rip current likelihoods as a function of incident wave height, period, direction, and spectral spread in frequency and direction over three bathymetries, including an alongshore uniform beach a moderately variable observed bathymetry

* Corresponding author.
E-mail address: jwchoi@kict.re.kr (J. Choi).

https://doi.org/10.1016/j.apor.2025.104727
Received 2 April 2025; Received in revised form 7 July 2025; Accepted 28 July 2025

(the Duck beach, NC, USA), and a strongly variable observed bathymetry (the Haeundae beach, South Korea). The FUNWAVE model was employed to resolve wave phases (i.e., a phase-resolving wave-current model) and simulate the vorticity induced by these phase-resolving wave-breaking forces (Peregrine, 1998), as well as to produce a rip-current risk index by using the likelihood distribution (Choi 2025).

Here, rip-current likelihood distributions on the three different beaches are explored to understand the relationship between wave parameters and alongshore bathymetric variations. The three bathymetries and the methodology for quantifying rip current likelihood through numerical simulations at each coast are described in Section 2, which details how to establish the likelihood distribution based on numerous FUNWAVE simulations. The 2-dimensional distributions of wave height-period, wave height-direction, wave height-frequency spreading, and wave height-directional spreading are presented in Section 3.

2. Methods

2.1. Bathymetries

The 3 bathymetries used to investigate rip current likelihoods include an idealized long straight beach (Fig. 1a), the observed alongshore inhomogeneous bathymetry with a sand bar at Duck, NC, USA (Fig. 1b), and a more complicated nearshore bathymetry featuring offshore rocks and reefs with pronounced alongshore variations observed in Haeundae, South Korea (Fig. 1c).

The Duck beach in October 2013 was selected due to its relatively moderate alongshore variability, whereas the Haeundae beach in Busan, located in southeastern Korea, was chosen for its strongly variable bathymetry and mega rip currents, triggered by summer swells from typhoons. These typhoons, originating in the Philippine and East China Seas and moving toward Taiwan and China, generate summer swells annually (Yoon et al. 2016). The bathymetry, characterized by offshore rocks and reefs with strong alongshore variations, significantly influences the generation of the mega rip currents (Shin et al. 2013).

2.2. Brief description of the FUNWAVE modeling

Here, a time-dependent phase-resolving wave and current model FUNWAVE that employs the fully nonlinear Boussinesq equations is used. The version of FUNWAVE (Chen et al. 2003) used contains a crucial improvement to previous versions (Wei et al. 1995) through the inclusion of a vortex force term. The equation for mass conservation can be written as

$$\eta_t + \nabla\cdot\boldsymbol{M} = 0, \tag{1}$$

where the subscript t denotes time differentiation, $\nabla = (\partial/\partial x, \partial/\partial y)$, and

$$\boldsymbol{M} = (h+\eta)\left\{\begin{array}{l}\boldsymbol{u}_\alpha + \left[\frac{z_\alpha^2}{2} - \frac{1}{6}(h^2 - h\eta + \eta^2)\nabla(\nabla\cdot\boldsymbol{u}_\alpha)\right] \\ \quad + \left[z_\alpha + \frac{1}{2}(h-\eta)\right]\nabla[\nabla\cdot(h\boldsymbol{u}_\alpha)]\end{array}\right\}, \tag{2}$$

where $\boldsymbol{M}$ is horizontal volume flux, h is the still water depth, η is the free surface elevation, and $\boldsymbol{u}_\alpha$ is the velocity vector at the reference elevation $z = z_\alpha = -0.53h$. The equation for momentum conservation is

$$\boldsymbol{u}_{\alpha t} + (\boldsymbol{u}_\alpha\cdot\nabla)\,\boldsymbol{u}_\alpha + g\nabla\eta + \boldsymbol{V}_1 + \boldsymbol{V}_2 + \boldsymbol{V}_3 - \boldsymbol{R}_b - \boldsymbol{R}_s + \boldsymbol{R}_f = 0, \tag{3}$$

where $\boldsymbol{V}_1$ and $\boldsymbol{V}_2$ are the dispersive Boussinesq terms, $\mathbf{V}_3$ accounts for the second-order effects of vertical vorticity, $\mathbf{R}_b$, $\mathbf{R}_s$, and $\mathbf{R}_f$ represent the effects of wave breaking, subgrid lateral turbulent mixing, and bottom friction, respectively. The numerical model has additional modules for practical applications, such as internal wave generation and absorbing layers (Chen et al. 1999; Chen et al. 2000; Kennedy et al. 2000). The version of FUNWAVE used here (version 2.0) recently has been applied in the context of harbor resonance (Gao et al. 2021; 2023; 2024).

The numerical model also has been used in studies of nearshore hydrodynamics with interactions between waves and currents (Chen et al. 1999, 2000; Johnson and Pattiaratchi 2006), and rip currents (Dalrymple et al. 2011). This model is well-suited for simulating transient rip currents (Johnson and Pattiaratchi 2006, Nuss et al. 2025), which are random in both time and location, as it simulates wave transformations, including the interference patterns of multidirectional random waves.

In addition, the model has been extensively validated with surfzone observations, including vorticity across multiple spatial scales, consistent with drifter dispersion (Spydell and Feddersen 2009), mean currents, eddy velocities, and tracer dispersion (Feddersen et al. 2011; Clark

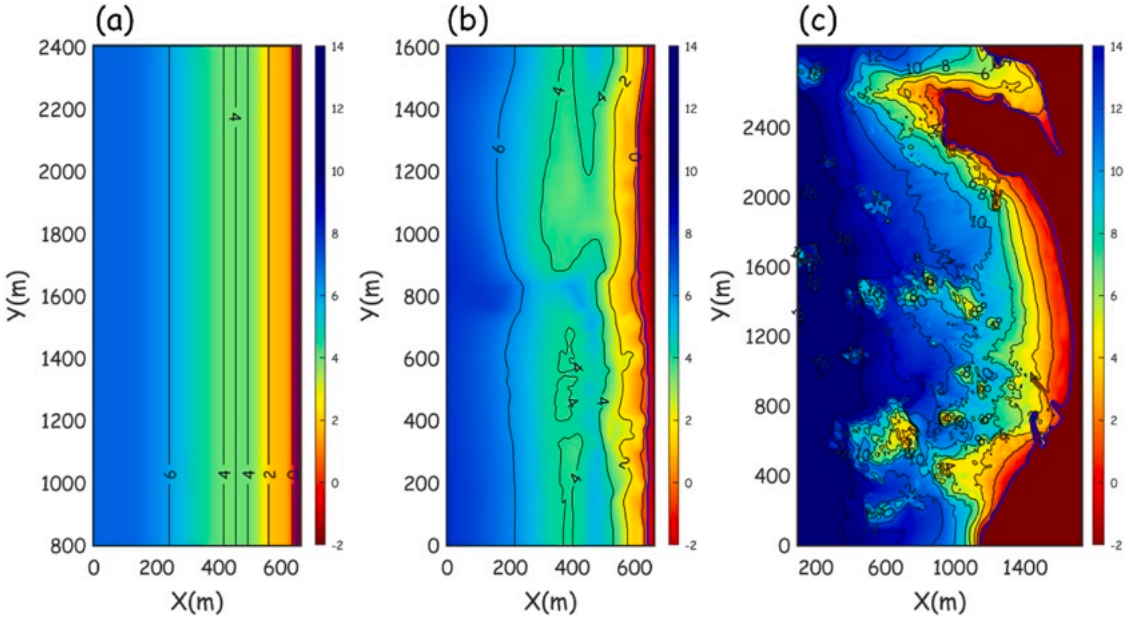

Fig. 1. Contours (scale on the right) and curves every 2 m of water depth of (a) a straight beach simplified using the Duck beach, (b) the Duck beach based on the survey of Oct., 2013, and (c) the Haeundae beach based on the survey of Nov., 2021 for the FUNWAVE modeling.

et al. 2011, and many others), and surfzone and inner-shelf exchange (Hally-Rosendahl and Feddersen 2016). Although these studies do not directly focus on rip currents, they validate essential hydrodynamic processes that contribute to their formation. FUNWAVE accurately simulates observed alongshore currents (Choi et al. 2015), and rip currents observed in the field at Haeundae Beach (Yoon et al. 2013) and in the laboratory (Choi and Roh 2021).

The model setup features periodic lateral boundaries, an absorption boundary, and a wavemaker boundary applied across the topography. The initial condition begins with still water as a cold start, and the boundary conditions are defined according to the coastal scenario outlined in the next section (Tables 2 and 3). The wave and tidal conditions were selected based on observed data, with the range of scenarios defined using evenly spaced intervals within realistic bounds. Extremely high wave conditions were excluded, considering both model limitations and the lack of swimmers during such conditions. The focus was placed on conditions where rip currents can pose hidden risks to beachgoers. The frequency spectrum was set in the range of 0.07-0.22 Hz with 25 frequency bands with varying bandwidth Δf and the spectrum had 41 directional bins with varying width $\Delta\theta$. Each bin corresponds to a discrete wave component with constant amplitude, associated with a specific frequency and angle of incidence. The spectrum was discretized using a constant-volume binning method (Kirby and Özkan 1994; Choi et al. 2015), which results in equal energy for each component. The grid sizes, the computational time step, the number of grids in the x and y directions of the simulations for the three bathymetries are shown in Table 1.

The values of all other parameters used in the numerical simulation were the same as those in previous studies (Choi et al. 2015), except for the use of a uniform friction coefficient f_c across the domain, chosen to avoid uncertainties associated with varying tidal ranges. For reference, the default coefficients for the initial and final threshold values ($\eta_t^{(I)}$ and $\eta_t^{(F)}$) that control the onset and cessation of wave breaking typically range from 0.35 to 0.65 for $\eta_t^{(I)}$, and are set to 0.15 for $\eta_t^{(F)}$. Here, $\eta_t^{(I)}$= 0.35 and $\eta_t^{(F)}$= 0.01 (Choi et al. 2015). A sensitivity analysis of rip current likelihood with respect to the FUNWAVE grid size, bottom friction factor, and wave breaking parameter is presented in the Appendix.

FUNWAVE calculates instantaneous velocities including wave-phase motions, and thus the rip current velocity is defined as the offshore-directed velocity averaged over two wave periods for each scenario. This short-term average better represents the conditions likely encountered by bathers when assessing rip current hazards. Averaging over longer time periods does not significantly alter the results (Appendix).

2.3. Quantification of rip-current likelihood

The rip-current likelihood for a given coastal scenario was determined as follows. A time series of the maximum offshore-directed flow velocity within the computational domain was obtained from the simulation results, representing the temporal variation of the maximum rip current velocity along the coast. The rip-current likelihood as a function of the variables i and j, $f_{i,j}$ (%) was estimated as the percent of the total time of intervals ($t_{v_{maxrip}>v_{danger}}$), in which the maximum rip current velocity (v_{maxrip}) is larger than a dangerous velocity (v_{danger}) set in advance, over the simulation time ($t_{simulation}$), yielding

$$f_{i,j} = \frac{1}{N}\left(\frac{t_{v_{maxrip}>v_{danger\_1}}}{t_{simulation}} + \frac{t_{v_{maxrip}>v_{danger\_2}}}{t_{simulation}} + \ldots + \frac{t_{v_{maxrip}>v_{danger\_N}}}{t_{simulation}}\right) \quad (4)$$

The dangerous velocity (v_{danger}) can be defined as an offshore-directed flow speed which could put swimmers in danger. The rip-current likelihood was estimated by averaging the percentages computed by using 0.5, 0.75, 1.0, 1.25, 1.5 m/s as the dangerous flow velocity (i.e., v_{danger_1}, v_{danger_2}, …, v_{danger_N}). The multiple speeds were employed rather than a single speed for the dangerous flow velocity, because the relationship between speed and danger in the surf zone varies widely depending on swimmer condition, such as age, physical ability, and use of floatation aides (e.g., life jackets, water wings). Although elite swimmers can reach speeds up to 1 m/s in still water, professional lifeguards have been measured at 0.7–0.9 m/s in the surf zone (Tipton et al. 2008). Average swimmers caught in rip currents typically swim at 0.2–0.4 m/s (Yuan et al. 2023). To study bather escape strategies from rip currents, a hazard rating based on velocity and depth (McCarroll et al. 2015; Castelle et al. 2016a) was developed through human stability experiments in floodwaters (RESCDAM, 2000; HR Wallingford, 2005), where a minimum or representative flow speed of 0.5 m/s is commonly applied. For example, time series of velocities for the observed Duck bathymetry (Fig. 2) suggest that rip current likelihoods increase as wave directions become more normally incident and narrower, as periods decrease, and as wave heights get larger (Table 2). A sensitivity analysis of rip current likelihood with respect to the selected threshold velocity is provided in the Appendix.

2.4. Scenarios for rip-current simulations

To derive the distributions of rip-current likelihood for a range of wave heights (H), wave periods (T), tidal elevations (E), wave directions (θ), frequency spectral spreading (F), and directional spectral spreading (D), numerical simulations were conducted with the input parameters over the three coasts (Tables 3 and 4). The spectral spreading parameter F (Goda, 1970) was defined as

$$F = \frac{2}{{m_0}^2}\int_0^\infty f\,{S_f}^2 df \quad (5)$$

where $m_n = \int_0^\infty f^n S_f df$, f is the wave frequency, S_f is the observed or forecast frequency spectrum, and the directional spreading parameter D (Longuet-Higgins et al., 1963) is defined as

$$D = \sqrt{dm_2/dm_0} \quad (6)$$

where $dm_n = \int_0^\infty\int_0^{2\pi} \theta^n S d\theta df$, θ is the wave direction, and S is the observed or forecast frequency-directional spectrum. The JONSWAP spectrum and the directional distribution (Mitsuyasu et al. 1975) were used for the input spectra in the simulations, with the parameters γ and σ_θ converted into the equations (5) and (6), respectively.

Boundary condition wave heights ranged from 0.7 to 1.7 m, peak wave periods from 5 to 15 s, with frequency spectra ranging from narrow (F=6) to broad (F=2), directions ranged from –40 to 40° relative to shore normal, with directional spreads ranging from narrow (D=0, i.e., uni-directional) to broad (D=35 deg), and tide-elevations from high (0.8 m MSL) to low (-0.8 m MSL) (Tables 3, 4). Additionally, for the Haeundae beach, which is known for its mega rip currents caused by summer swells, monochromatic wave simulations were conducted using the input conditions from Table 4 excluding the spectral spreads.

Table 1
Grid sizes (Δx, Δy), the computational time step (Δt), the number of grids in the x and y directions of the simulations for the three bathymetries, including the straight beach, the Duck beach, and the Haeundae beach.

Site	Grid size (m) and time step (s)			Number of grids	
	Δx	Δy	Δt	x (cross shore)	y (alongshore)
Straight beach	1.5	2.0	0.05	441	1601
Duck beach	1.5	2.0	0.05	441	801
Haeundae beach	1.2	1.8	0.05	1551	1678

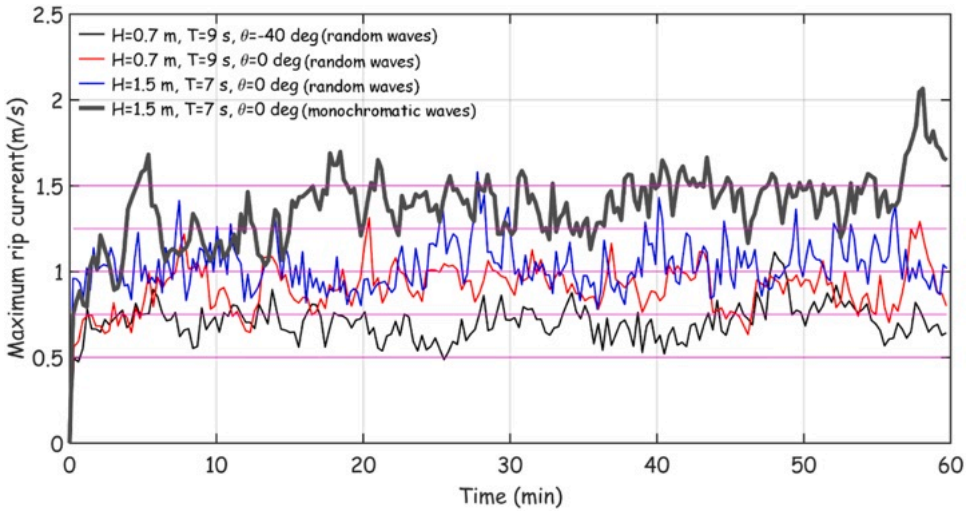

Fig. 2. Maximum (averaged over 2 wave periods) rip current velocity versus time in the simulations listed in Table 2 using the observed Duck bathymetry (Fig. 1b). The initial conditions for the curves are described in the legend. The horizontal magenta lines indicate the threshold (of danger) velocities to calculate the corresponding rip-current likelihoods.

Table 2
The rip-current likelihoods obtained from the time series of the FUNWAVE simulation results based on the observed Duck beach (Fig. 1b). The likelihood represents the average percent of flows averaged over 2 wave periods exceeding dangerous velocities of 0.5, 0.75, 1.0, 1.25, and 1.5 m/s.

No	Height (m)	Period (s)	Direction (deg)	Tide (m, MSL)	Frequency Spreading (γ)	Directional Spreading (σ_θ)	Likelihood (%)
1	0.7	9	40	0.0	9.9	20	18
2	0.7	9	0	0.0	9.9	20	38
3	1.5	7	0	0.0	9.9	20	51
4	1.5	7	0	0.0	Monochromatic		83

Table 3
Wave and tidal conditions as the inputs for numerical simulations of random wave-induced rip currents using the straight (Fig. 1a) and the observed (Fig. 1b) Duck beach. The elevation is at MSL datum, the angle 0° indicates normally incident waves, and the parentheses for the 9 s waves indicate the number of cases varied with each parameter.

T H	5s	7s	9s		11s	13s	15s
0.7m	θ=0° E=0m F=6.0 D=21°	θ=0° E=0m F=6.0 D=21°	E=0m, D=21°,F=6.0, -40≤θ≤40° (10) θ=0°, D=21°,F=6.0, -0.8≤E≤0.8m (7)	θ=0°, E=0m, D=21°, 2≤ F ≤6 (5) θ=0°, E=0m, F=6, 0°≤ D ≤ 35°(7)	θ=0° E=0m F=6.0 D=21°	θ=0° E=0m F=6.0 D=21°	θ=0° E=0m F=6.0 D=21°
0.9m	θ=0° E=0m F=6.0 D=21°	θ=0° E=0m F=6.0 D=21°	E=0m, D=21°,F=6.0, -40≤θ≤40° (10) θ=0°, D=21°,F=6.0, -0.8≤E≤0.8m (7)	θ=0°, E=0m, D=21°, 2≤ F ≤6 (5) θ=0°, E=0m, F=6, 0°≤ D ≤ 35°(7)	θ=0° E=0m F=6.0 D=21°	θ=0° E=0m F=6.0 D=21°	θ=0° E=0m F=6.0 D=21°
1.1m	θ=0° E=0m F=6.0 D=21°	θ=0° E=0m F=6.0 D=21°	E=0m, D=21°,F=6.0, -40≤θ≤40° (10) θ=0°, D=21°,F=6.0, -0.8≤E≤0.8m (7)	θ=0°, E=0m, D=21°, 2≤ F ≤6 (5) θ=0°, E=0m, F=6, 0°≤ D ≤ 35°(7)	θ=0° E=0m F=6.0 D=21°	θ=0° E=0m F=6.0 D=21°	θ=0° E=0m F=6.0 D=21°
1.3m	θ=0° E=0m F=6.0 D=21°	θ=0° E=0m F=6.0 D=21°	E=0m, D=21°,F=6.0, -40≤θ≤40° (10) θ=0°, D=21°,F=6.0, -0.8≤E≤0.8m (7)	θ=0°, E=0m, D=21°, 2≤ F ≤6 (5) θ=0°, E=0m, F=6, 0°≤ D ≤ 35°(7)	θ=0°, E=0m, 2≤ F ≤6 0°≤ D ≤ 35° (35)	θ=0° E=0m F=6.0 D=21°	θ=0° E=0m F=6.0 D=21°
1.5m	θ=0° E=0m F=6.0 D=21°	θ=0° E=0m F=6.0 D=21°	E=0m, D=21°,F=6.0, -40≤θ≤40° (10) θ=0°, D=21°,F=6.0, -0.8≤E≤0.8m (7)	θ=0°, E=0m, D=21°, 2≤ F ≤6 (5) θ=0°, E=0m, F=6, 0°≤ D ≤ 35°(7)	θ=0° E=0m F=6.0 D=21°	θ=0° E=0m F=6.0 D=21°	θ=0° E=0m F=6.0 D=21°
1.7m	θ=0° E=0m F=6.0 D=21°	θ=0° E=0m F=6.0 D=21°	E=0m, D=21°,F=6.0, -40≤θ≤40° (10) θ=0°, D=21°,F=6.0, -0.8≤E≤0.8m (7)	θ=0°, E=0m, D=21°, 2≤ F ≤6 (5) θ=0°, E=0m, F=6, 0°≤ D ≤ 35°(7)	θ=0° E=0m F=6.0 D=21°	θ=0° E=0m F=6.0 D=21°	θ=0° E=0m F=6.0 D=21°

The likelihood distributions of wave height and period (H,T), wave height-direction (H,θ), wave height-tidal elevation (H,E), wave height-frequency spectral spreading (H,F), wave height-direction spectral spreading (H,D), and wave frequency-direction spectral spreading (F,D), were obtained by quantifying rip-current likelihood from the simulations.

The numerical simulations include 263 cases for each scenario: the straight beach and the Duck beach, and 268 cases for the Haeundae

Table 4
Scenario of wave and tidal conditions as the inputs for numerical simulations of random wave-induced rip currents using the Haeundae beach (Fig. 1c). The elevation is at MSL datum, the angle 0° indicates normally incident waves, and the parentheses indicate the number of cases varied with each parameter.

T H	5s	7s	9s	11s		13s	15s
0.7m	θ=0° E=-0.6m F=6.0 D=16°	θ=0° E=-0.6m F=6.0 D=16°	θ=0° E=-0.6m F=6.0 D=16°	E=-0.6m, D=16°,F=6.0, -40≤θ≤40° (10) θ=0°, D=16°,F=6.0, -0.8≤E≤0.8m (7)	θ=0°, E=-0.6m, D=16°, 2≤ F ≤6 (5) θ=0°, E=0m, F=6, 0°≤ D ≤ 35°(7)	θ=0° E=-0.6m F=6.0 D=16°	θ=0° E=-0.6m F=6.0 D=16°
0.9m	θ=0° E=-0.6m F=6.0 D=16°	θ=0° E=-0.6m F=6.0 D=16°	θ=0° E=-0.6m F=6.0 D=16°	E=-0.6m, D=16°,F=6.0, -40≤θ≤40° (10) θ=0°, D=16°,F=6.0, -0.8≤E≤0.8m (7)	θ=0°, E=-0.6m, 2≤ F ≤6 0°≤ D ≤ 35° (35)	θ=0° E=-0.6m F=6.0 D=16°	θ=0° E=-0.6m F=6.0 D=16°
1.1m	θ=0° E=-0.6m F=6.0 D=16°	θ=0° E=-0.6m F=6.0 D=16°	θ=0° E=0m F=6.0 D=16°	E=-0.6m, D=16°,F=6.0, -40≤θ≤40° (10) θ=0°, D=16°,F=6.0, -0.8≤E≤0.8m (7)	θ=0°, E=-0.6m, D=16°, 2≤ F ≤6 (5) θ=0°, E=0m, F=6, 0°≤ D ≤ 35°(7)	θ=0° E=-0.6m F=6.0 D=16°	θ=0° E=-0.6m F=6.0 D=16°
1.3m	θ=0° E=-0.6m F=6.0 D=16°	θ=0° E=-0.6m F=6.0 D=16°	θ=0° E=0m F=6.0 D=16°	E=-0.6m, D=16°,F=6.0, -40≤θ≤40° (10) θ=0°, D=16°,F=6.0, -0.8≤E≤0.8m (7)	θ=0°, E=-0.6m, D=16°, 2≤ F ≤6 (5) θ=0°, E=0m, F=6, 0°≤ D ≤ 35°(7)	θ=0° E=-0.6m F=6.0 D=16°	θ=0° E=-0.6m F=6.0 D=16°
1.5m	θ=0° E=-0.6m F=6.0 D=16°	θ=0° E=-0.6m F=6.0 D=16°	θ=0° E=-0.6m F=6.0 D=16°	E=-0.6m, D=16°,F=6.0, -40≤θ≤40° (10) θ=0°, D=16°,F=6.0, -0.8≤E≤0.8m (7)	θ=0°, E=-0.6m, D=16°, 2≤ F ≤6 (5) θ=0°, E=0m, F=6, 0°≤ D ≤ 35°(7)	θ=0° E=-0.6m F=6.0 D=16°	θ=0° E=-0.6m F=6.0 D=16°
1.7m	θ=0° E=-0.6m F=6.0 D=16°	θ=0° E=-0.6m F=6.0 D=16°	θ=0° E=-0.6m F=6.0 D=16°	E=-0.6m, D=16°,F=6.0, -40≤θ≤40° (10) θ=0°, D=16°,F=6.0, -0.8≤E≤0.8m (7)	θ=0°, E=-0.6m, D=16°, 2≤ F ≤6 (5) θ=0°, E=-0.6m, F=6, 0°≤ D ≤ 35°(7)	θ=0° E=-0.6m F=6.0 D=16°	θ=0° E=-0.6m F=6.0 D=16°

beach, requiring approximately 120 days under a single-node configuration using 6 PCs (96 cores) equipped with Intel i7 CPUs and 32 GB of RAM (each case took less than 20 days to run on a single core).

3. Results

3.1. Samples of the FUNWAVE simulations

The simulation results for the alongshore uniform coast (Fig. 1a) under the scenario of H_s=1.3 m, T_s=13 s, with normally incident waves at mean sea level, with γ=9.9 and σ_θ=20° (i.e., F=6 and D=21°) at the offshore boundary show that the directionally spread waves (Fig. 3a) break nonuniformly (Fig. 3b) along the straight sandbar, generating vorticity (Fig. 3c), and rip currents (Fig. 3d).

The simulation results for the observed Duck beach (Fig. 1b) for H_s=1.4 m, T_s=7 s with normally incident waves at mean sea level, with γ=9.9 and σ_θ=20° (i.e., F=6 and D=21°) at the offshore boundary included alongshore variability of the incoming short-crested waves (Fig. 4a) that broke non-uniformly on the alongshore varying bathymetry (Fig. 4b), generating vorticity (Fig. 4c) and relatively strong rip

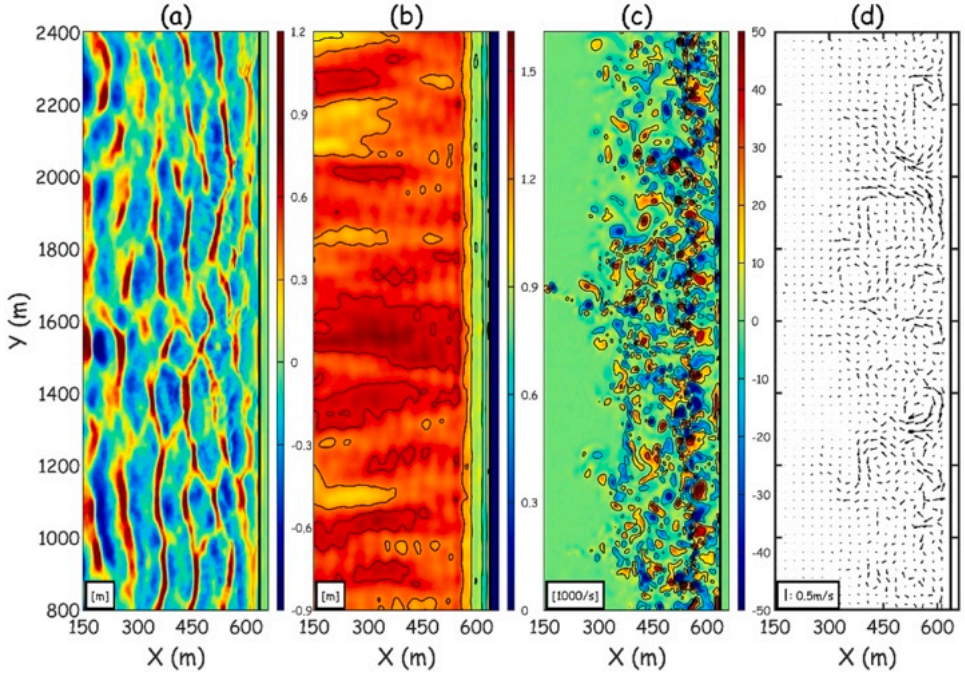

Fig. 3. Contours (color scales on the right of each panel) as a function of alongshore and cross-shore coordinate for simulations on the straight beach (Fig. 1a) for (a) surface displacement (m) at t=100 T_s, (b) wave height (m) averaged over 0≤t≤150 T_s, (c) vorticity (1000/s), and (d) current vectors (m/s) at t=100 T_s, for H_s=1.3 m, T_s=13 s, with normally incident waves at mean sea level, with γ=9.9 and σ_θ=20°(i.e., F=6 and D=21°).

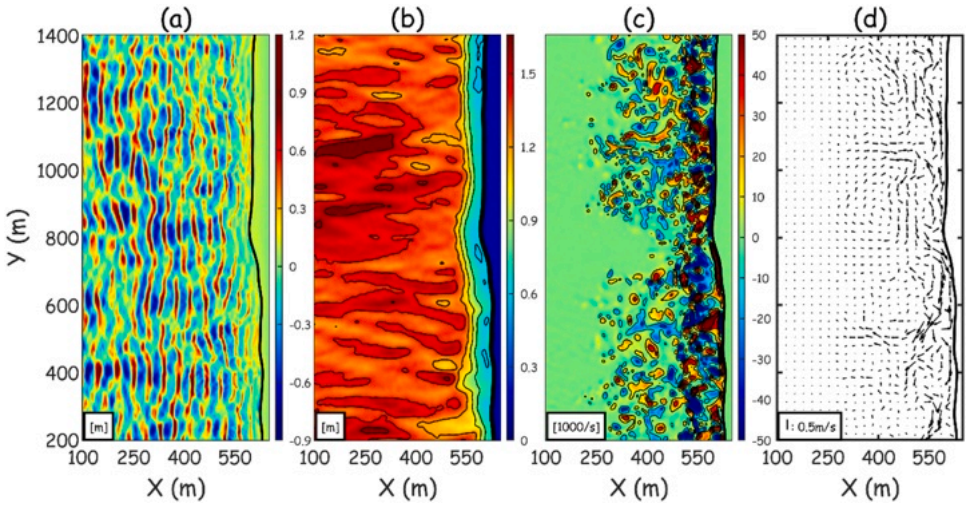

Fig. 4. Contours (color scales on the right of each panel) as a function of alongshore and cross-shore coordinate for simulations on the alongshore nonuniform observed bathymetry at Duck (Fig. 1b), showing (a) surface displacement (m) at t=100 T_s, (b) wave height (m) averaged over $0 \leq t \leq 150$ T_s, (c) vorticity (1000/s), and (d) current vectors (m/s) at t=100 T_s, for H_s=1.4 m, T_s=7 s, with normally incident waves at mean sea level, with γ=9.9 and σ_θ=20°(i.e., F=6 and D=21°).

currents (Fig. 4d).

The simulation results for the Haeundae coast, which includes natural headlands at its lateral ends and some subsea outcrops and reefs outside the surf zone (Fig. 1c) for H_s=1.1 m, T_s=11 s, with normally incident waves at mean sea level, and with γ=9.9 and σ_θ=15° (i.e., F=6 and D=16°) produced strongly spatially variable waves (Fig. 5a), and breaking (Fig. 5b), with strong rip currents (Fig. 5d).

3.2. Distributions of rip current likelihood

Rip current likelihood varied according to wave height and wave period at each of the coasts for normally incident, directionally spread waves (Fig. 6) and for monochromatic waves (Fig. 7) on the observed bathymetries. The likelihood distributions denote that the rip current likelihood increases as wave height increases, with the maxima occurring for different periods for the three topographies (Fig. 6). Rip current likelihoods decrease with longer periods over the alongshore uniform bathymetry of the straight coast (Fig. 6a), likely owing to the shorter crests of the higher frequency waves with the same directional spreading involving stronger alongshore variability of the wave field. Rip current likelihoods increase for 10 to 12 s waves over the observed bathymetry of the Duck beach (Fig. 6b), owing to alongshore variations in bathymetry, as well as to alongshore variability of incident wave field. Rip current likelihoods also increase with longer wave periods over the strong alongshore variation in bathymetry of the Haeundae coast (Fig. 6c). The likelihoods on the straight beach and the observed Duck bathymetry partially are higher than those on the Haeundae coast during short-crested incident waves (i.e., directionally spread waves), especially with the shorter wave periods. The variability of the wave field due to directionally spread incident waves might affect the alongshore straight (Fig. 1a) and moderately variable (Fig. 1b) beaches more than the more highly variable bathymetry of the Haeundae beach (Fig. 1c).

The simulations suggest that the rip currents for monochromatic waves (Fig. 7) are stronger than those for the broad-in-frequency waves with the equivalent wave height (Fig. 6). As a result, the complicated coast tends to have larger rip current likelihoods during narrow-band swell. Rip current likelihood should be zero for normally incident monochromatic swell propagating across alongshore uniform bathymetry. For monochromatic waves, likelihoods increase with decreasing

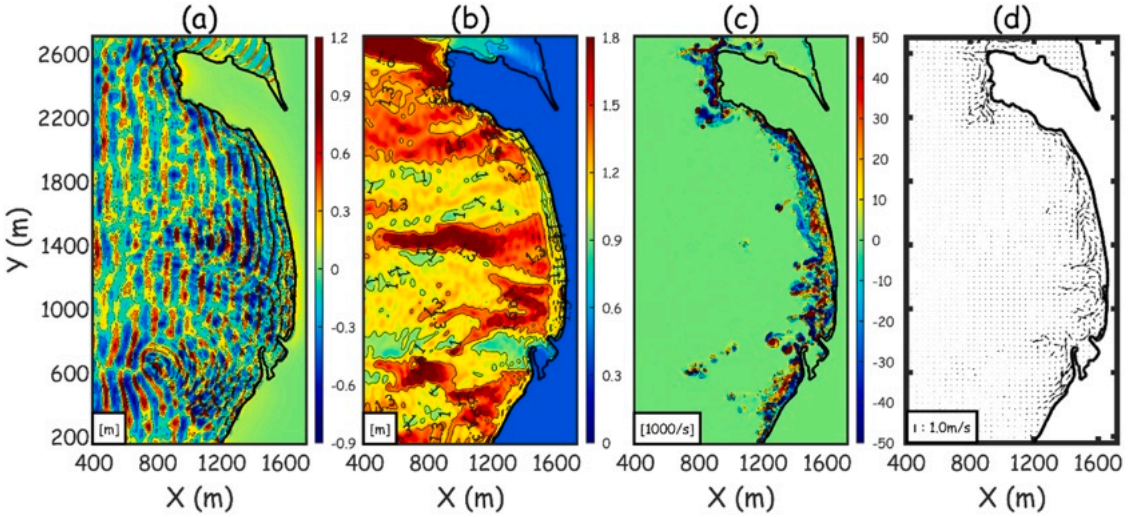

Fig. 5. Contours (color scales on the right of each panel) as a function of alongshore and cross-shore coordinate for simulations on the spatially complex nearshore at Haeundae (Fig. 1c), for (a) surface displacement (m) at t=100 T_s, (b) wave height (m) averaged over $0 \leq t \leq 150$ T_s, (c) vorticity (1000/s), and (d) current vectors (m/s) at t=100 T_s, for H_s=1.1 m, T_s=11 s with incident waves from the south at -0.6 m relative to mean sea level, with γ=9.9 and σ_θ=15° (i.e., F=6 and D=16°).

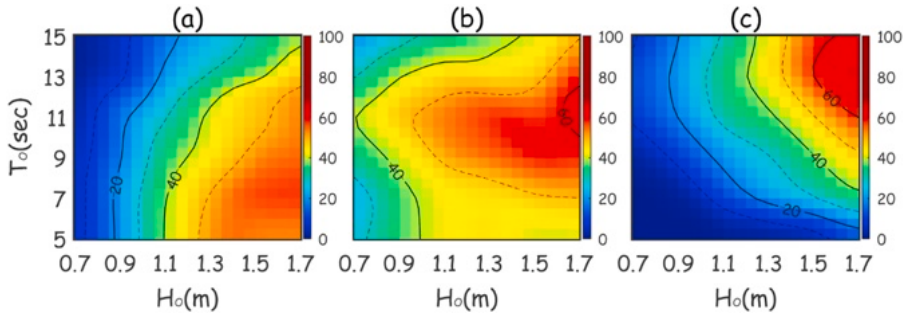

Fig. 6. Contours (color scales on the right sides with curves every 20%) of rip current likelihood f_{HT}(%) as a function of wave period and significant wave height for (a) the straight beach (θ=0°, E=0 m, F=6, D=21°(γ=9.9 and σ_θ=20°)), (b) the Duck beach (θ=0°, E=0 m, F=6, D=21°(γ=9.9 and σ_θ=20°)), and (c) the Haeundae beach (θ=0°, E=-0.4 m, F=6, D=16°(γ=9.9 and σ_θ=15°)).

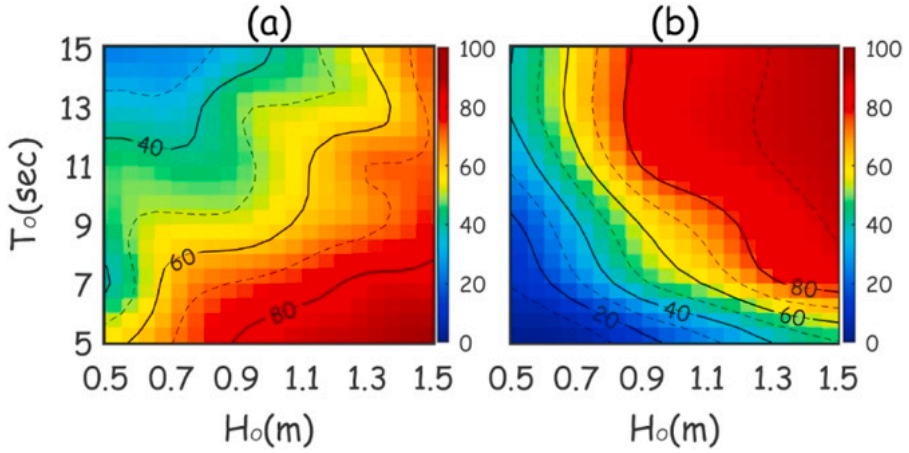

Fig. 7. Contours (color scales on the right sides with curves every 20%) of rip current likelihood f_{HT}(%) as a function of wave period and significant wave height for (a) the observed Duck bathymetry (monochromatic waves with θ=0°, E=0 m,) and (b) the Haeundae beach (monochromatic waves with θ=0°, E=-0.6 m).

wave period on the Duck bathymetry (Fig. 7a), whereas likelihoods increase with increasing wave period on the more variable bathymetry of Haeundae (Fig. 7b). The likelihoods for Haeundae for directionally spread (Fig. 6c) and directionally narrow (Fig. 7b) wave fields are similar, likely because the strong alongshore bathymetric variability results in alongshore variations in the waves as they shoal, refract, and break on the complex bathymetry.

Rip current likelihood is affected by the direction of the incoming waves, with normally incident waves more likely to generate rip currents (Fig. 8), with the likelihood increasing with wave height. As incident waves arrive at large angles relative to shore normal, the momentum of the associated breaking-wave-induced mean alongshore currents is such that cross-shore flows are suppressed (Moulton et al. 2017). For the straight coast the likelihoods for the largest oblique wave directions (e.g., 40°) are higher than for the less oblique directions (e.g., 20°) (Fig. 8a), possibly an artifact of the generation of shear waves from the strong alongshore currents shedding eddies with offshore directed currents. Shear instabilities in the alongshore current can generate surf zone eddies (Feddersen 2014 and many others) that are more likely to develop on alongshore-uniform beaches when exposed to highly oblique wave conditions (Castelle et al. 2016b). On the more complicated Haeundae coast, monochromatic waves result in high likelihoods for a wide range of incident directions (Fig. 8c).

On the straight beach (Fig. 1a) likelihoods are highest for low tides (shallower water depths, Fig. 9a). In contrast, on the observed Duck bathymetry (Fig. 1b) the highest likelihoods occur near mid tide

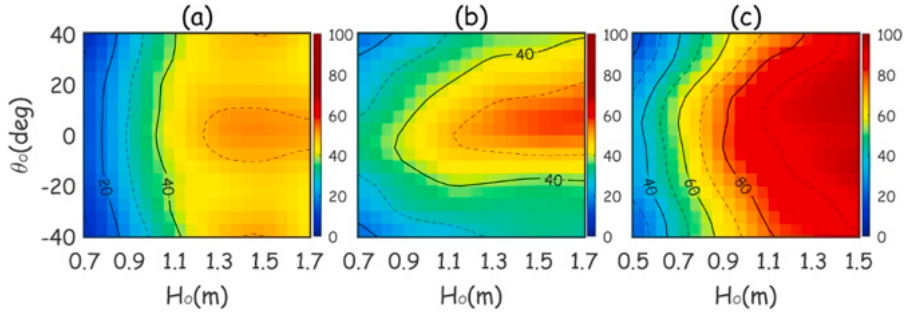

Fig. 8. Contours (color scales on the right sides with curves every 20%) of rip current likelihood $f_{H\theta}$(%) as a function of wave direction relative to normal and significant wave height for (a) the straight beach (T=9 s, E=0 m, F=6, D=21°(γ=9.9 and σ_θ=20°)), (b) the observed Duck bathymetry (T=9 s, E=0 m, F=6, D=21° (γ=9.9 and σ_θ=20°)), and (c) the Haeundae beach (T=11 s, E=-0.6 m with monochromatic waves).

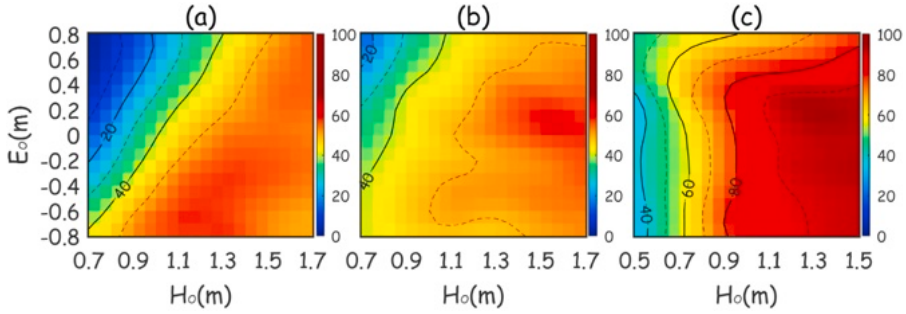

Fig. 9. Contours (color scales on the right sides with curves every 20%) of rip current likelihood f_{HE}(%) as a function of tidal elevation and significant wave height for (a) the straight beach (T=9 s, θ=0°, F=6, D=21°(γ=9.9 and σ_θ=20°)), (b) the observed Duck bathymetry (T=9 s, θ=0°, F=6, D=21°(γ=9.9 and σ_θ=20°)), and (c) the Haeundae beach (T=11 s, θ=0° with monochromatic waves).

(Fig. 9b), and on the Haeundae coast likelihoods are similar for almost all tidal stages (Fig. 9c). These aspects are attributed to alongshore variability and changes in cross-shore slope influenced by tidal stages, with particular attention to the artificial modifications at the Haeundae coast following beach nourishments (Choi, 2022).

For the Haeundae coast (Figs. 6–7), the rip current likelihoods under monochromatic wave conditions were higher than those under random waves, although the overall spatial patterns were similar. A similar trend was observed in the effects of different wave directions and tidal elevations (not shown). Therefore, the results under monochromatic wave conditions were presented (Figs. 8–9), because they produce stronger rip currents on the complex bathymetry.

As the bandwidth of the power spectrum decreases, the likelihoods increase for all three bathymetries (Fig. 10), although the increase is smaller for the Haeundae coast (Fig. 10c) than the other two coasts (Figs. 10a,b). The likelihoods are lower for the straight beach (Fig. 10a) than the other two coasts (Figs. 10b,c), and likelihoods are highest for Haeundae even though the incident waves have smaller directional spread (σ_θ=15°) than for the Duck beach (σ_θ=20°), suggesting that for broad-band wave fields bathymetric variations increase the likelihood of rip currents.

Likelihoods increase as the directional spectrum gets wider on the straight (Fig. 11a) and Duck (Fig. 11b) beaches, but not on the Haeundae coast (Fig. 11c) where the strong bathymetric variations tend to dominate over the effects of the width of the directional spectrum.

On the straight and observed Duck beaches, likelihoods increase as the directional spread increases and the width of the power spectrum decreases (Figs. 12 a,b). Likelihoods are similar on the more variable Haeundae bathymetry, except for low directional spread with narrow-band frequency spectra (Fig. 12c), which produce the highest likelihoods. This is attributed to the successive ends of wave crests and the associated offshore-directed flows, generated by the complex offshore rocks and reefs under incident wave fields characterized by narrow frequency and directional spread (Shin et al. 2013).

4. Summary and discussion

The likelihood of rip currents was investigated with a Boussinesq numerical wave model (FUNWAVE) run over three nearshore bathymetries, including an alongshore uniform beach, observed sandbar morphology at Duck, NC, USA, and the complicated nearshore area observed at Haeundae beach in South Korea. In the simulations, rip current likelihood increases as incident wave heights increase, as has been shown in many previous studies. As the bathymetry becomes more variable, the highest likelihoods occur for longer period, directionally spread incident waves (except for Haeundae beach), with normally incident waves producing the highest likelihoods, as also has been shown previously. The highest likelihoods occur for low tides (shallow water), although the effect of water depth is small for the most complicated bathymetry. Narrow frequency spectra result in the highest likelihoods of rip currents, with the effect decreasing as the bathymetry becomes more variable. As the directional spread increases so does the rip current likelihood, except for the most variable bathymetry where likelihood decreases slightly as the directional spread increases. The simulations suggest that as the bathymetry becomes more complex, the likelihood of rip currents becomes increasingly dominated by the associated shoaling, refracting, and breaking than by the details of the incident wave field characteristics.

The distribution in this study does not account for bathymetric changes in the surf zone, particularly during and after storms, due to the lack of a morphological change model. These changes significantly affect rip current dynamics, warranting future research on how distributions vary with storm-induced bathymetric evolution. Bathymetric evolution observed over a short period (~1 week) can lead to noticeable changes (up to ~20%) in rip current likelihoods under identical wave conditions (Choi and Elgar, 2025).

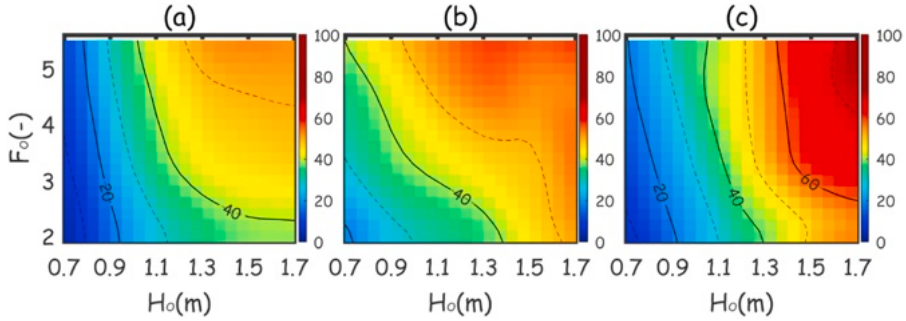

Fig. 10. Contours (color scales on the right sides with curves every 20%) of rip current likelihood f_{HF}(%) as a function of power spectral bandwidth and significant wave height for (a) the straight beach (T=9 s, θ=0°, E=0 m, and D =21°(σ_θ=20°)), (b) the observed Duck bathymetry (T=9 s, θ=0°, E=0 m, and D=21°(σ_θ=20°)), and (c) the Haeundae beach (T=11 s, θ=0°, E=-0.4 m, and D=16°(σ_θ=15°)).

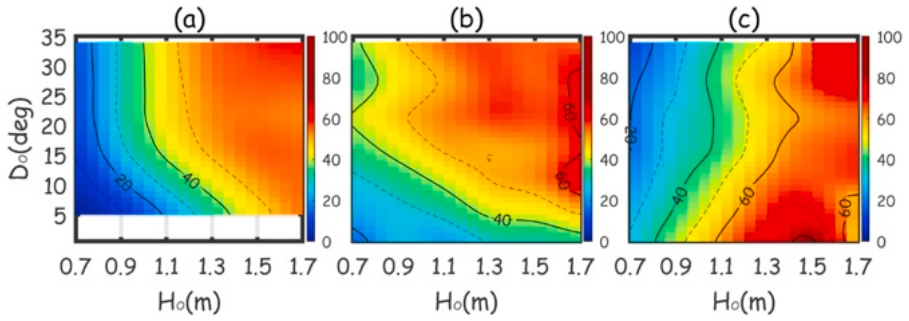

Fig. 11. Contours (color scales on the right sides with curves every 20%) of rip current likelihood f_{HD}(%) as a function of bandwidth of the directional spectrum and significant wave height for (a) the straight beach (T=9 s, θ=0°, E=0 m, and F=6(γ=9.9)), (b) the observed Duck bathymetry (T=9 s, θ=0°, E=0 m, and F=6(γ=9.9)), and (c) the Haeundae beach (T=11 s, θ=0°, E=-0.4 m, and F=6(γ=9.9)).

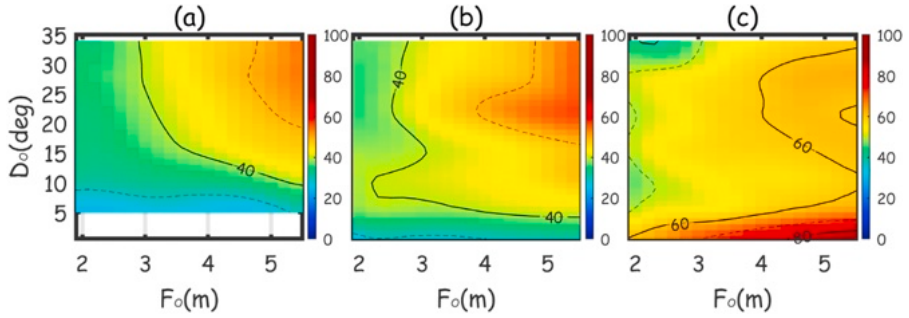

Fig. 12. . Contours (color scales on the right sides with curves every 20%) of rip current likelihood f_{FD}(%) as a function of bandwidth of the directional spectrum and significant wave height for (a) the straight beach (H=1.3 m, T=11 s, θ=0°, and E=0 m), (b) the observed Duck bathymetry (H=1.3 m, T=11 s, θ=0°, and E=0 m), and (c) the Haeundae beach (H=0.9 m, T=11 s, θ=0°, and E=-0.4 m).

Additionally, artificial incident wave coherence was implemented by the wave maker (Salatin et al. 2021). However, if bathymetric variations are significant, they will become the dominant controlling factor, even though the variability of the wave field increases with the degree of wave coherence for an alongshore uniform beach. Whereas Haeundae Beach exhibited minimal sandbar variability, but significant intermediate water depth variation, Sandcity Beach (Geiman et al. 2011) showed substantial sandbar variability. To improve the generalizability of the findings, future studies should consider a broader set of beach types, including those with varying degrees of alongshore variability and bar configurations. Although the present study provides a theoretical framework for estimating rip current likelihoods, its application to real-time forecasting remains to be developed.

CRediT authorship contribution statement

Junwoo Choi: Writing – original draft, Visualization, Validation, Resources, Methodology, Investigation, Funding acquisition, Formal analysis, Data curation, Conceptualization. **Steve Elgar:** Writing – review & editing, Writing – original draft, Data curation, Conceptualization. **James T. Kirby:** Writing – review & editing, Software.

Declaration of competing interest

The authors declare the following financial interests/personal relationships which may be considered as potential competing interests:

Steve Elgar reports financial support was provided by US National Science Foundation. Junwoo Choi reports financial support was provided by Korea Hydrographic and Oceanographic Agency. If there are other authors, they declare that they have no known competing financial interests or personal relationships that could have appeared to influence the work reported in this paper.

Acknowledgements

Funding was provided by the Ministry of Oceans and Fisheries, the Korea Hydrographic and Oceanographic Agency of Republic of Korea, and the US National Science Foundation.

Appendix

This appendix discusses the sensitivity of rip current likelihood to the choice of FUNWAVE grid size, bottom friction factor, and wave breaking parameter, the impact of the selected time-averaging period (e.g., two wave periods) on the nearshore current velocity derived from FUNWAVE, and the sensitivity to the choice of threshold velocity.

To assess the sensitivity of the results to the FUNWAVE grid size, wave breaking parameter, and bottom friction coefficient, three additional simulations were conducted using alternative values. The baseline FUNWAVE simulations use a grid size of Δx=1.5m, Δy=2.0m, a bottom friction factor of f_c=0.0015, and a breaking parameter c_{br1}=0.35 for $\eta_t^{(I)}$. In the sensitivity tests, all other conditions remained the same, except for: (1) an increased friction coefficient f_c=0.003 (Fig. A1a); (2) a finer grid size of Δx=1.2, Δy=1.5 m (Fig. A1b); and (3) a larger breaking parameter c_{br1}=0.5 for $\eta_t^{(I)}$(Fig. A1c).

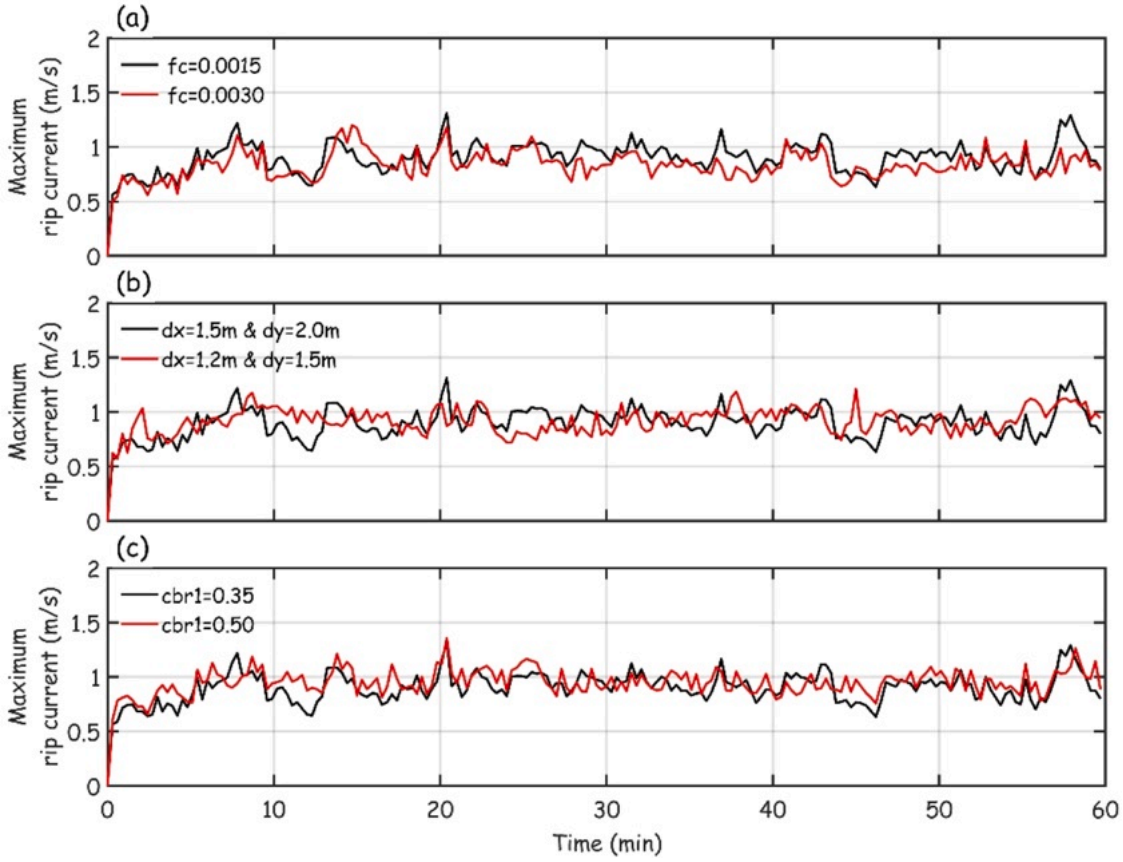

Fig. A1. Maximum (averaged over 2 wave periods) rip current versus time in the simulations for H_s=0.7 m, T_s=9 s, with normally incident waves at mean sea level, with γ=9.9 and σ_θ=20°(i.e., F=6 and D=21°) (Table 2) using the observed Duck bathymetry (Fig. 1b). The FUNWAVE inputs for the curves are described in the legend.

The baseline FUNWAVE simulation resulted in a rip current likelihood of 38%, whereas the additional test cases (1)–(3) yielded likelihoods of 31%, 40%, and 43%, respectively. Increasing the friction factor reduces the rip current likelihood, whereas increasing the breaking parameter enhances it. Additionally, using a finer grid, which reduces numerical dissipation, slightly increases the rip current likelihood. Although a comprehensive analysis across numerous scenarios would be required to explore nonlinear parameter interactions, the current results suggest parameter variations shift likelihood values ~10%. Consequently, these adjustments are unlikely to significantly alter the overall spatial patterns of rip current likelihood compared with changes driven by wave and tidal parameters.

The impact of the selected time-averaging period was evaluated using velocities averaged over 2, 20, and 50 wave periods (Fig. A2). The maximum offshore-directed velocity at x=~561, y=~552 m is about 0.9 m/s for averaging over 2 periods (Fig. A2a) and 0.7 m/s for 50 periods (Fig. A2c). These results indicate that the rip current velocities and their overall patterns similar across different averaging periods. The 2-period average was selected because that is a current a swimmer in danger will experience.

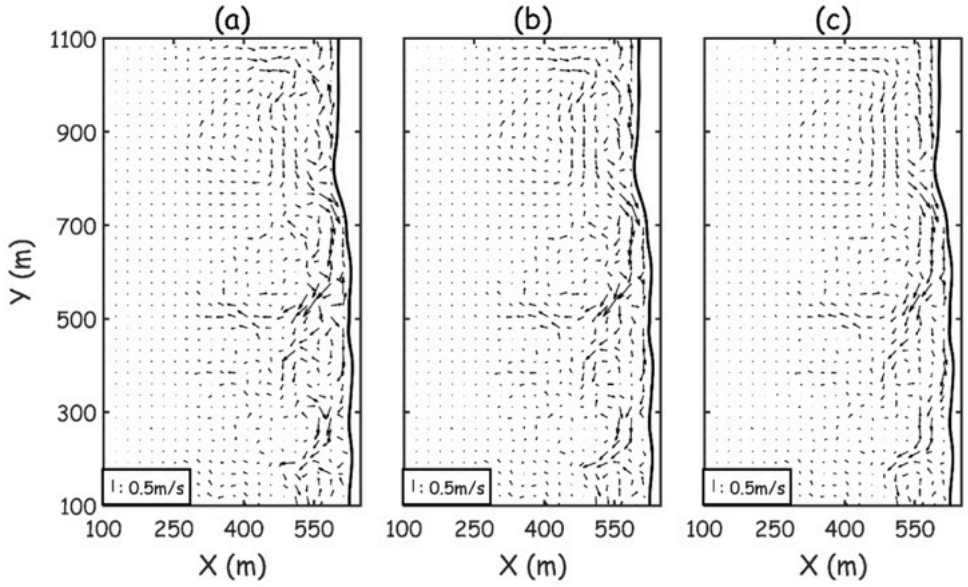

Fig. A2. Nearshore current vectors (m/s) derived from FUNWAVE as a function of alongshore and cross-shore coordinates for (averages over (a) 2T (~13s), (b) 20T (~67s), and (c) 50T (~335s) at t=200 T_o, for H_o=1.4m, T_o=6.7s, with normally incident waves at mean sea level, with γ=9.9 and σ_θ=20° using the observed Duck bathymetry (Fig. 1b).

Previous FUNWAVE studies of surf zone flows and eddy dynamics have averaged over 30 s (Hally-Rosendahl and Feddersen 2016, alongshore currents and dye concentration), 300 s (Geiman and Kirby, 2013, rip currents), and two-weeks (Choi et al. 2015, time-varying alongshore currents).

Rip current likelihoods f_{HT}(%) as a function of wave period and significant wave height were computed for the observed Duck beach using threshold velocities of 0.6, 0.9, and 1.2 m/s (Fig. A3). As the threshold velocity for danger increases, the likelihood decreases (Fig. A3). Although averaging likelihoods across multiple thresholds simplifies the representation of rip current hazards, it provides a generalized evaluation applicable across diverse swimmer abilities.

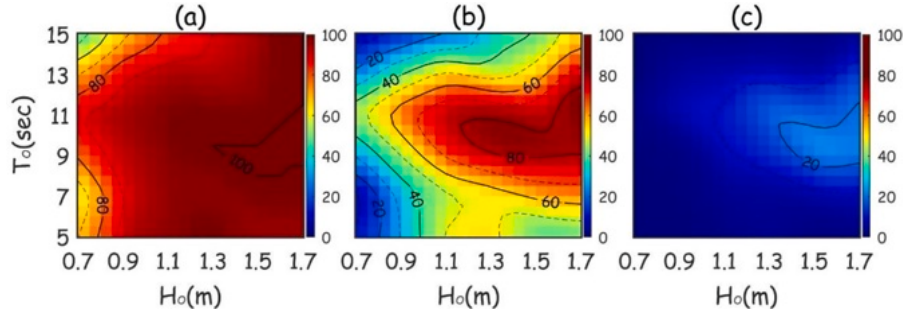

Fig. A3. Contours (color scales on the right sides with curves every 20%) of rip current likelihood f_{HT}(%) as a function of wave period and significant wave height for the observed Duck beach (Figure 1b) (θ=0°, E = 0 m, F = 6, D=21° (γ=9.9 and σ_θ=20°)) with threshold velocities v_{danger} of (a) 0.6, (b) 0.9, and (c) 1.2 m/s.

References

Akan, Ç., McWilliams, J.C., Uchiyama, Y., 2020. Topographic and coastline influences on surf eddies. Ocean Modell. 147, 101565.

Bowen, A.J., 1969. Rip currents: 1. Theoretical investigations. J. Geophysic. Res. 74 (23), 5467–5478.

Castelle, B., McCarroll, R.J., Brander, R.W., Scott, T., Dubarbier, B., 2016a. Modelling the alongshore variability of optimum rip current escape strategies on a multiple rip-channelled beach. Nat. Hazards 81, 663–686.

Castelle, B., Scott, T., Brander, R.W., McCarroll, R.J., 2016b. Rip current types, circulation and hazard. Earth-Sci. Rev. 163, 1–21.

Chen, Q., Dalrymple, R., Kirby, J.T., Kennedy, A., Haller, M., 1999. Boussinesq modelling of a rip current system. J. Geophys. Res. 104, 20617–20637.

Chen, Q., Kirby, J.T., Dalrymple, R.A., Kennedy, A., Chawla, A., 2000. Boussinesq modeling of wave transformation, breaking and runup, *II: 2d.* J. Wtrwy., Port, Coast. Ocean Eng. 126 (1), 48–56.

Chen, Q., Kirby, J.T., Dalrymple, R.A., Shi, F., Thornton, E.B., 2003. Boussinesq modeling of longshore current. J. Geophys. Res. 108 (C11), 26-1-26-18.

Choi, J., 2022. A numerical study on rip currents at the Haeundae coast changed after the beach nourishment. J. Korea Water Resour. Associat. 55 (9), 669–678 in Korean.

Choi, J., 2025. A rip-current prediction/forecast model employing likelihoods of rip currents beforehand simulated by a phase-resolving wave-current model. Ocean Eng. 331, 121153.

Choi, J., Elgar, S., 2025. Rip current likelihoods and predictions on 2 different bathymetries observed within 1 week on the same beach in Duck, NC. Weather Forecast under review.

Choi, J., Kirby, J.T., Yoon, S.B., 2015. Boussinesq modeling of longshore currents in the SandyDuck experiment under directional random wave conditions. Coastal Eng 101, 17–34.

Choi, J., Lim, C.H., Yoon, S.B., 2013. A rip current warning system based on real-time observations for Haeundae Beach, Korea. J. Coast. Res. SI 72, 56–62.

Choi, J., Roh, M., 2021. A laboratory experiment of rip currents between the ends of breaking wave crests. Coast. Eng. 164, 103812.

Clark, D.B., Feddersen, F., Guza, R.T., 2011. Modeling surfzone tracer plumes, part 2: transport and dispersion. J. Geophysic. Res. 116, C11028.

Dalrymple, R.A., MacMahan, J.H., Reniers, A.J.H.M., Nelko, V., 2011. Rip currents. Annu. Rev. Fluid Mech. 43, 551–581.

Dusek, G., Seim, H., 2013a. Rip current intensity estimates from lifeguard observations. J. Coastal Res. 29 (3), 505–518.

Dusek, G., Seim, H., 2013b. A probabilistic rip current forecast model. J. Coast. Res. 29 (4), 909–925.

Feddersen, F., 2014. The generation of surfzone eddies in a strong alongshore current. J. Phys. Oceanogr. 44, 600–617.

Feddersen, F., Clark, D.B., Guza, R.T., 2011. Modeling surfzone tracer plumes, part 1: waves, mean currents, and low-frequency eddies. J. Geophysic. Res. 116, C11027.

Gao, J., Ma, X., Dong, G., Chen, H., Liu, Q., Zang, J., 2021. Investigation on the effects of Bragg reflection on harbor oscillations. Coast. Eng. 170, 103977.

Gao, J., Shi, H., Zang, J., Liu, Y., 2023. Mechanism analysis on the mitigation of harbor resonance by periodic undulating topography. Ocean Eng. 281, 114923.
Gao, J., Hou, L., Liu, Y., Shi, H., 2024. Influences of Bragg reflection on harbor resonance triggered by irregular wave groups. Ocean. Eng. 305, 117941.
Geiman, J.D., Kirby, J.T., 2013. Unforced Oscillation of Rip-Current Vortex Cells. J. Physical Ocean. 43, 477–497.
Geiman, J.D., Kirby, J.T., Reniers, A.J.H.M., MacMahan, J.H., 2011. Effects of wave averaging on estimates of fluid mixing in the surf zone. J. Geophysic. Res. 116, C04006. https://doi.org/10.1029/2010JC006678.
Gensini, V.A., Ashley, W.S., 2009. An examination of rip current fatalities in the United States. Nat. Hazard. 54 (1), 159–175.
Goda, Y., 1970. Numerical experiments on wave statistics with spectral simulation, *report of the Port and Harbour Research Institute*, 8, Nagase, Japan.
Haller, M.C., Dalrymple, R.A., 2001. Rip current instabilities. J. Fluid Mech. 433, 161–192.
Hally-Rosendahl, K., Feddersen, F., 2016. Modeling surfzone to inner-shelf tracer exchange. J.F Geophys. Res 121, 8888–8909.
HR Wallingford, 2005. R&D outputs: flood risks to people, phase 2, FD2321/TR1, the Risks to people methodology.
Johnson, D., Pattiaratchi, C., 2006. Boussinesq modelling of transient rip currents. Coast. Eng 53, 419–439.
Kennedy, A.B., Chen, Q., Kirby, J.T., Dalrymple, R.A., 2000. Boussinesq modeling of wave transformation, breaking, and runup, *I: 1D*. J. Wtrwy. Port, Coast. Ocean Eng. 126, 39–47.
Kirby, J.T., Özkan, H.T., 1994. Combined refraction/diffraction model for spectral wave conditions. Center for Applied Coastal Research, Dept. of Civil Engineering, University of Delaware, Newark, DE, p. 33.
Longuet-Higgins, M.S., Cartwright, D.E., Smith, N.D., 1963. Observations of the directional spectrum of sea waves using the motions of a floating buoy. Ocean wave spectra. Prentice-Hall, Englewood Cliffs, New Jersey, pp. 111–136.
MacMahan, J.H., Reniers, A.J., Thornton, E.B., Stanton, T.P., 2004. Infragravity rip current pulsations. J. Geophysic. Res. 109, C01033.
McCarroll, R.J., Castelle, B., Brander, R.W., Scott, T., 2015. Modelling rip current flow and bather escape strategies across a transverse bar and rip channel morphology. Geomorphology 246, 502–518.
Mitsuyasu, H., Tasai, F., Suhara, T., Mizuno, S., Ohkusu, M., Honda, T., Rikiishi, K., 1975. Observations of the directional spectrum of ocean waves using a cloverleaf buoy. J. Physic. Oceanograph. 5, 750–760.
Moulton, M., Elgar, S., Raubenheimer, B., Warner, J.C., Kumar, N., 2017. Rip currents and alongshore flows in single channels dredged in the surf zone. J. Geophysic. Res. 122. https://doi.org/10.1002/2016JC012222.
NOAA, National Oceanic and Atmospheric Administration, 2022a. Weather related fatality and injury statistics, National Weather Service, Available at weather.gov/hazstat/(Accessed: September 1, 2022).
Nuss, E.S., Moulton, M., Suanda, S.H., Baker, C.M., 2025. Modeled surf-zone eddies on a laboratory scale barred beach with varying wave conditions. J. Geophysic. Res. 130, e2023JC020549. https://doi.org/10.1029/2023JC020549.
O'Dea, A., Kumar, N., Haller, M.C., 2021. Simulations of the surf zone eddy field and cross-shore exchange on a nonidealized bathymetry. J. Geophysic. Res. 126, e2020JC016619.
Peregrine, D.H., 1998. Surf zone currents. Theoretic. Computat. Fluid Dynam 10, 295–309.
RESCDAM, 2000. The use of physical models in dam-break flood analysis. Final Report of Helsinki University of Technology data, December 2000. Appendix 2 to Final Report of RESCDAM, June 2001.
Salatin, R., Chen, Q., Bak, A.S., Shi, F., Brandt, S.R., 2021. Effects of wave coherence on longshore variability of nearshore wave processes. J. Geophysic. Res. 126, e2021JC017641.
Shin, C.H., Roh, H.K., Yoon, S.B., Choi, J., 2013. Understanding of rip current generation mechanism at Haeundae Beach of Korea: honeycomb waves. J. Coast. Res. SI72, 11–15.
Spydell, M., Feddersen, F., 2009. Lagrangian drifter dispersion in the surf zone: directionally spread, normally incident waves. J. Physic. Oceanogr. 39 (4), 809–830.
Suanda, S.H., Feddersen, F., 2015. A self-similar scaling for cross-shelf exchange driven by transient rip currents. Geophysic. Res. Lett. 42, 5427–5434.
SLS, Surf Life Saving, 2022. Coastal safety report 2022, Available at beachsafe.org.au/surf-safety/ripcurrents(Accessed: January 1, 2023).
Tang, E.-S., Dalrymple, R.A., 1989. Nearshore circulation: rip currents and wave groups. Advances in Coastal and Ocean Engineering. Plenum Press, New York, pp. 205–230.
Tipton, M., Reilly, T., Rees, A., Spray, G., Golden, F., 2008. Swimming performance in surf: the influence of experience. Int. J. Sports Med. 29 (11), 895–898.
Uchiyama, Y., McWilliams, J.C., Akan, C., 2017. Three-dimensional transient rip currents: bathymetric excitation of low-frequency intrinsic variability. J. Geophysic. Res. 122, 5826–5849.
Yoon, S.B., Park, W.K., Choi, J., 2013. Observation of rip current velocity at an accidental event by using video image analysis. J. Coast. Res. SI 72, 16–21.
Yoon, S.B., Song, J-H, Roh, M., Choi, J., 2016. Rip currents generated by distant typhoons at Haeundae Beach of Korea: forecast and warning. J. Coast. Res. SI (75), 1417–1421.
Yuan, Y., Yang, H., Yu, F., Gao, Y., Li, B., Xing, C., 2023. A wave-resolving modeling study of rip current variability, rip hazard, and swimmer escape strategies on an embayed beach. Nat. Hazards Earth Syst. Sci. 23, 3367–3384.
Wei, G., Kirby, J., Grilli, S.T., Subraymanya, R., 1995. A fully non-linear Boussinesq model for surface waves: i. Highly non-linear unsteady waves. J. Fluid Mech. 294, 71–92.